Available online at www.sciencedirect.com
ScienceDirect
Journal of Power Sources 162 (2006) 66–73
JOURNAL OF POWER SOURCES
www.elsevier.com/locate/jpowsour

Structure of Pt/C and PtRu/C catalytic layers prepared by plasma sputtering and electric performance in direct methanol fuel cells (DMFC)

A. Caillard [a], C. Coutanceau [b,*], P. Brault [a], J. Mathias [a], J.-M. Léger [b]

[a] *Groupe de Recherche sur l'Energétique des Milieux Ionisés, UMR6606 Université d'Orléans, CNRS, Polytech'Orléans BP6744, F-45067 Orléans Cedex 2, France*
[b] *Laboratoire de Catalyse en Chimie Organique, UMR6503 Université de Poitiers, CNRS, F-86022 Poitiers, France*

Received 29 May 2006; received in revised form 19 June 2006; accepted 1 July 2006
Available online 15 September 2006

Abstract

Plasma sputtering process was used to deposit Pt and PtRu on conductive carbon diffusion layer. Low metal loading catalysts for methanol electrooxidation were prepared and characterized by TEM and XRD. The main result is that codeposition of Pt and Ru leads to alloy phase, whereas multi-layers deposition leads to no-alloyed structure. The electrochemical performance of sputtered Pt/C electrodes was compared with that of standard electrodes, and was found lower. However, the specific activity was much higher, indicating that the catalyst utilization efficiency was higher than that obtained with a standard electrode. Then, different bimetallic PtRu/C electrodes were prepared by plasma sputtering, leading to different catalyst structures (Pt and Ru multilayer deposition or simultaneous deposition of Pt and Ru) and composition (from 100:0 to 50:50 Pt/Ru atomic ratios). At last, the different PtRu electrodes were compared in term of DMFC electrical performance. The best efficiency of the DMFC was reached when both metals Pt and Ru are simultaneously deposited (alloyed) with a ruthenium atomic ratio of 30% or 40 % Ru depending of the working potentials of the cell.

Keywords: DMFC; Methanol oxidation; Plasma sputtering deposition; Platinum; Ruthenium

1. Introduction

Proton exchange membrane fuel cells (PEMFC) are promising power sources for many applications, such as automotive [1,2], portable [3–5] or stationary applications [6,7]. Although significant targets have been overcome during the two last decades [8], further researches are necessary for decreasing the cost of the fuel cell, keeping good efficiency. For example hydrogen as fuel in a polymer electrolyte membrane fuel cell (PEMFC) leads to high electric efficiency; however its production and storage are still problematic [9–11]. Direct supply of a fuel cell with liquid fuels like alcohols in direct alcohol fuel cells (DAFC) appears then advantageous for two main reasons: easy storage and handling, and a relatively high theoretical specific energy (6.1 and 8.0 kWh kg^{-1} for methanol and ethanol, respectively [12]). However, one of the main problems for direct methanol fuel cell (DMFC) is the slow electrooxidation kinetics due to CO poisoning of the platinum catalytic surface, coming from the dissociative adsorption of MeOH [13,14]. As a result, complete oxidation of methanol in CO_2 occurs at high overvoltages, where CO species can effectively be oxidized. This leads to a drastic decrease in electrical performance of a DMFC. In order to decrease the poisoning of catalysts, ruthenium is often added to platinum. Its role is explained by the combination of two effects: the so-called bifunctional mechanism [15] where partially oxidized ruthenium surface procure oxygenated species necessary to complete the oxidation of methanol adsorption residue to CO_2, and the ligand effect [16,17] where ruthenium atoms close to platinum are expected to influence the density of electronic states of platinum leading to the weakening the Pt–CO bond [18]. However, to achieve acceptable electrical performance of the DMFC, high loading of PtRu catalyst is needed (typically close to 1.0–2.0 mg_{PtRu} cm^{-2} catalyst). Despite of this, the electrical performance of a DMFC does not reach that of a PEMFC working with catalysts loading 5–10 times lower. Improvements of the catalysts structure are still needed.

* Corresponding author. Tel.: +33 5 49 45 48 95; fax: +33 5 49 45 35 80.
E-mail address: christophe.coutanceau@univ-poitiers.fr (C. Coutanceau).

0378-7753/$ – see front matter © 2006 Elsevier B.V. All rights reserved.
doi:10.1016/j.jpowsour.2006.07.009

DMFC electrodes are generally prepared by brushing, spraying or printing an ink of liquid Nafion® and carbon supported catalyst dispersed in a solvent [19–27]. Electrodeposition [28–31] and sputtering seem good alternatives to reduce the catalysts loading on fuel cell electrodes [25,32]. All these processes are widely used for Pt deposition on Nafion® membrane or on diffusion layer (DL) for PEM fuel cell. In the last decade, Brault et al. [32] and Hirano et al. [33] achieved equivalent electrical performance with a H_2/O_2 PEMFC working with plasma sputtered Pt/C electrodes (loading of 0.10 $mg_{Pt}\,cm^{-2}$) than with standard electrodes. Recently, Cha and Lee [34,35] and Haug et al. [36] achieved electrical performance with about 40 $\mu g_{Pt}\,cm^{-2}$ loading electrodes close to that obtained with electrodes of higher platinum loading (close to 0.5 $mg\,cm^{-2}$). The electrodes were prepared by alternatively sputtering platinum layers (5 nm) and applying Nafion® and carbon ink layers directly on the membrane. However, in the field of DMFC, a few works is reported in the literature [37,38].

In this work, platinum and bimetallic platinum–ruthenium catalysts are prepared using plasma sputtering process on conductive carbon diffusion layer (DL). Several deposition methods of platinum and ruthenium were tested: co-deposition and alternative deposition of Pt and Ru, leading to different catalyst structures and compositions. Their electrochemical performances were then compared under DMFC working conditions with that of standard electrodes.

2. Experimental

2.1. Chemically prepared cathode

Colloidal precursors are synthesized according to the procedure described by Bönnemann et al. [39], but slightly modified. All experiments were carried out under argon, using anhydrous salts and dry solvents. Reducing agent $N^+(C_nH_{2n+1})_4[BEt_3H]^-$ is prepared by mixing stoichiometric amounts of tetraalkylamonium bromide $[N^+(C_nH_{2n+1})_4Br^-]$ and potassium triethylborohydride $[K(BEt_3H)]$ in tetrahydrofuran (THF). While added to this solution, the metallic salts ($PtCl_2$ from Alfa Aesar) were reduced according to the following reaction:

$$PtCl_2 + 2N^+(C_nH_{2n+1})_4[BEt_3H]^- \rightarrow Pt[N^+(C_nH_{2n+1})_4Cl^-]_2 + 2BEt_3 + H_2 \quad (1)$$

The colloidal precursors were dispersed onto a high specific area carbon substrate (Vulcan XC72). The carbon supported metal powders were then prepared by thermal treatment of these precursors at 300 °C under air for 1 h. The platinum particles were found to have a mean diameter close to 2.7 nm which is in agreement with previous results [40,41].

Homemade electrodes were prepared from ink composed of a Nafion® solution (5 wt.% from Aldrich), the desired amount of catalytic powder and isopropanol as solvent, brushed on a carbon diffusion layer (DL). DL was homemade using a carbon cloth from Electrochem Inc. on which was brushed ink made of Vulcan XC72 carbon powder and PTFE dissolved in isopropanol. The gas diffusion electrodes were loaded with 3.5 $mg\,cm^{-2}$ of a mixture of carbon powder and 30 wt.% PTFE. The metal loading of chemical electrodes (called standard electrodes in the text) was close to 2 $mg\,cm^{-2}$ and the Nafion® loading was 0.8 $mg\,cm^{-2}$.

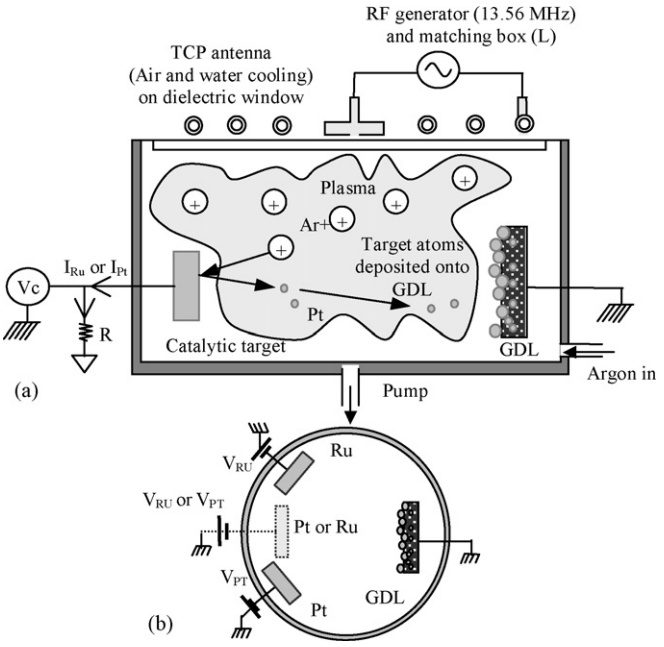

Fig. 1. Schema of the plasma sputtering reactor: (a) side view (b) top view (single and dual target configuration).

2.2. Plasma sputtered catalyst on anodic DL

Anodic catalysts were deposited by plasma sputtering on the same DL than above. The low-pressure plasma set-up is described in Fig. 1. More details are given in previous works [32,42]. To proceed the sputtering, the platinum (and/or ruthenium) target(s) faced the DL in a vacuum reactor. Briefly, the biased target is sputtered by energetic argon ions created by inductive plasma excited by a planar coil through a dielectric window (transformer coupled plasma (TCP) antenna). The antenna is powered by a RF generator (13.56 MHz, 1000 W). All electrodes were prepared with the same Ar working pressure (0.5 Pa) and target-substrate distance (5.5 cm). Because different parameters are adjustable (one or two target, deposition time, power...), the plasma sputtering technique is very powerful to prepare catalysts with different structure and atomic ratios. Sputtered electrodes were prepared either by simultaneous deposition of ruthenium and platinum (catalysts PtRu1–5) or by deposition of Ru on Pt coated DL (catalyst 2L-PtRu1 and 2) or 10 alternative depositions of Pt and Ru on DL (catalyst 10L-PtRu1 and 2). For Pt and Ru co-deposition the power supply for the platinum target and ruthenium target are simultaneously and independently adjusted between 100 and 300 V in order to obtain the desired atomic composition of catalysts. For double-layer and multi-layer PtRu catalysts, a power supply of 200 W was used, leading to a deposition rate of 14 $\mu g\,cm^{-2}\,min^{-1}$ for platinum and 5.5 $\mu g\,cm^{-2}\,min^{-1}$ for ruthenium. The deposition time was modulated in order to obtain

Table 1
Preparation, number of layers, weight composition and atomic ratio of the sputtered platinum based catalysts

Sputtered catalyst sample name	Preparation	Composition (mg cm^{-2})	Atomic ratio
Pt/C			
Pt1	1 layer	0.17	–
Pt2		0.08	–
Pt3		0.04	–
Pt4		0.03	–
PtRu codeposition			
PtRu1	1 layer	Pt: 0.32; Ru: 0.02	90:10
PtRu2		Pt: 0.26; Ru: 0.03	80:20
PtRu3		Pt: 0.31; Ru: 0.07	70:30
PtRu4		Pt: 0.30; Ru: 0.09	60:40
PtRu5		Pt: 0.33; Ru: 0.17	50:50
PtRu multi-layers			
2L-PtRu2	2 layers	Pt: 0.4; Ru: 0.06	80:20
2L-PtRu4		Pt: 0.4; Ru: 0.13	60:40
10L-PtRu2	10 layers	Pt: 0.29; Ru: 0.04	80:20
10L-PtRu4		Pt: 0.28; Ru: 0.09	60:40

desired atomic compositions. All prepared catalysts are given in Table 1 with their number of layers, weight composition and atomic ratio.

Coated gas diffusion layers (called gas diffusion electrodes) were analysed by high resolution scanning electronic microscopy (SEM) and transmission electron microscopy (TEM) to reveal their morphology. Rutherford backscattering spectroscopy (RBS) was used to measure the deposition rate of platinum and ruthenium and to determinate the catalyst densities and depth profile in the porous DL.

The crystallographic microstructure of the catalytic powders was investigated by X-ray diffraction (XRD). Powder X-ray diffraction patterns were recorded using a Brucker D5005 with a secondary monochromator and a scintillation detector, for the characterization of catalysts. The apparatus is in the Bragg–Brentano geometry and work with the Cu wavelength λ, Cu $K\alpha_1$–α_2, i.e. Cu $K\alpha_1 = 1.54060$ Å and Cu $K\alpha_2 = 1.54443$ Å. Unfortunately, the estimation of the crystallites sizes was not realizable without introducing great uncertainty, because of the presence and contribution in the whole pattern of carbon and PTFE.

2.3. Fuel cell tests

Standard cathodes (2.0 mg_{Pt} cm^{-2} loading, 40 wt.% metal/C, 40 wt.% PTFE, 0.8 mg cm^{-2} Nafion®) were used in the MEAs (membrane electrode assemblies). On the other hand, anodes were made by wetting the sputtered PtRu/C electrodes with a mixture of Nafion® 5 wt.% solution from Aldrich and water, in order to obtain a Nafion® loading of 0.8 mg cm^{-2}.

To ensure good contact between the components, the MEAs were prepared by hot pressing (130 °C, 90 s, under a pressure of 35 kg cm^{-2}) a pre-treated Nafion® 117 membrane with a standard cathode on one side and a sputtered anode on the other side. Results are compared to a MEA with a standard anode (Pt loading 2 mg cm^{-2}) as a reference.

The fuel cell tests were carried out with a single 5 cm^2 DMFC using a Globe Tech test bench. The temperature was set at 90 °C for the fuel cell and 95 °C for the oxygen humidifier. The pressures of methanol and oxygen were set to 2 and 3 bar, respectively. The polarization curves E versus j and power density curves P versus j curves were recorded using a high power potentiostat (Wenking model HP 88) interfaced with a PC to apply the current sequences and to store the data, and a variable resistor in order to fix the applied current to the cell.

The same batches of Nafion® membranes, Nafion® solution and Vulcan XC 72 was used within each series of measurements.

3. Results and discussion

3.1. Catalyst deposition morphology

The deposition morphology (mean particles size) of the platinum and ruthenium nanoparticles were first examined after direct deposition on separate microscopy grids (300 meshes copper grid) coated with a carbon film. The platinum and ruthenium loading was (4.10^{15} atoms cm^{-2}) leading to 1.3 μg_{Pt} cm^{-2} and 0.66 μg_{Ru} cm^{-2}, respectively. The apparent mean size of metallic particles was evaluated using TEM microscopy (Fig. 2a and b for platinum and ruthenium, respectively). Platinum and ruthenium nanoparticles deposited on non-porous carbon film display bean shapes with mean sizes close to 2.9 and 2.2 nm for platinum particles and ruthenium particles, respectively. The mean diameter of Ru particles dispersed on carbon film is smaller for the same atomic loading. Similar fact was already observed between nanodispersed particles of platinum and ruthenium synthesised following the Bönnemann method: TEM and DRX characterization of Pt (30 wt.%)/C catalysts and Ru(30 wt.%)/C gave apparent mean particles sizes of 2.2 and 1.5, respectively [43].

The morphology and structure of platinum nanoparticles deposited on a carbon diffusion layer (DL) was examined by

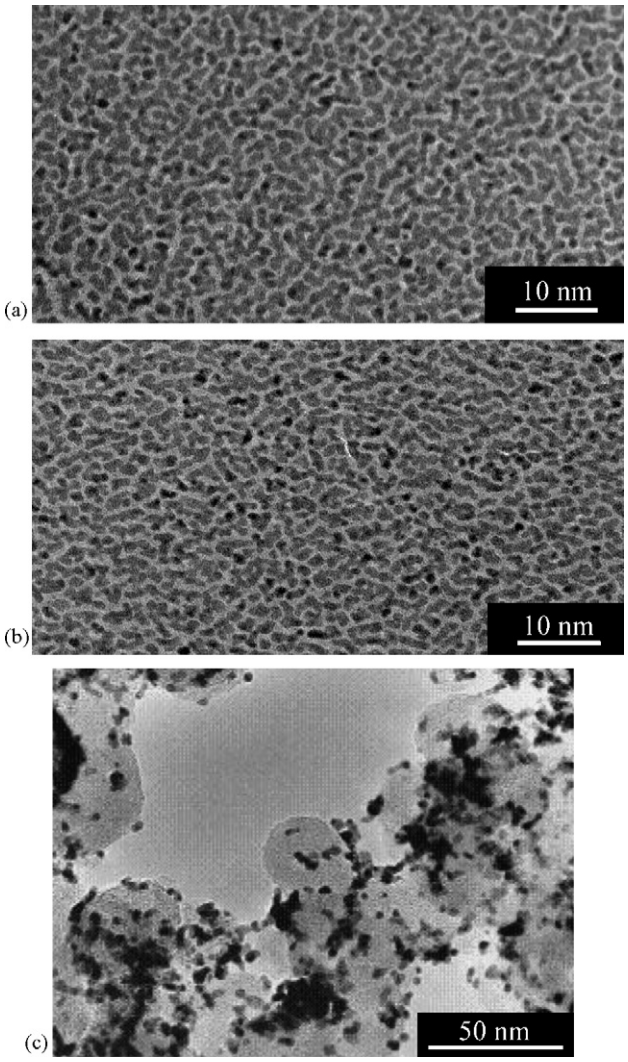

Fig. 2. TEM images of nanoparticles deposited by plasma sputtering ($5\,\mu g_{Pt/Ru}\,cm^{-2}$); (a) platinum deposited on a carbon film, (b) ruthenium deposited on a carbon film and (c) platinum deposited on deposition on carbon DL. Power generator: 100 W; target bias: −300 V; pressure: 0.5 Pa; current on catalytic target: 20 mA; distance target-DL: 5.5 cm.

transmission electron microscopy. Such DL, on which some anhydrous drops had been poured, was lightly rubbed with a microscopy grid (300 meshes copper grid coated by Lacey carbon membrane). Fig. 2c shows the micrograph of platinum particles dispersed on carbon Vulcan XC 72 support corresponding to a metal loading of $5\,\mu g\,cm^{-2}$. The formation of aggregates with sizes between 8 and 10 nm is evidenced. These aggregates are in fact composed of smaller particles with an average size of the particles close to 3.0 nm. The deposition of platinum on porous carbon diffusion layer does not induce change in the mean apparent size of platinum nanoparticles (2.9 and 3.0 nm, for platinum deposited on a carbon film and on a carbon DL, respectively). However, agglomeration of nanoparticles in clusters of 8–10 nm starts to occur on carbon DL even for so low platinum loading. For higher metal loadings (typically greater than $20\,\mu g_{Pt}\,cm^{-2}$), a thin platinum film surrounding carbon particles is formed, as shown in Fig. 3. This platinum thin film, which is formed on the top surface of the carbon DL, may have

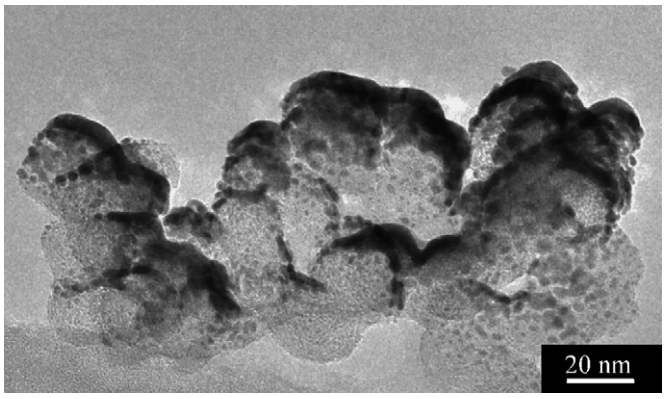

Fig. 3. TEM image of platinum nanoparticules ($20\,\mu g\,cm^{-2}$) Pt and thin film deposited by plasma sputtering on the carbon particles of a DL. Power generator: 100 W; target bias: −300 V; pressure: 0.5 Pa; current on catalytic target: 20 mA; distance target-DL: 5.5 cm.

some role in electrocatalytic activity towards methanol oxidation (see next section).

On the other hand, it is a very challenging experimental problem to determine the structure and morphology of bimetallic catalysts prepared by simultaneous or mutlti-layer deposition of platinum and ruthenium. Here, the use of X-ray diffraction method could give some information concerning the PtRu particles structure (Pt surrounded by smaller Ru particles or PtRu alloy particles or. . .). According to the Vegard's law for a true PtRu alloy, the value of the cell parameter must decrease when the ruthenium content increases. In other words, the diffraction peaks shift towards higher 2θ value when ruthenium is alloyed with platinum [44]. XRD patterns of standard Pt/C, of commercial PtRu (1:1)/C, of 10L-PtRu4/C catalyst and of PtRu4/C catalysts are represented in Fig. 4. All diffraction patterns display the typical diffraction peaks of the fcc structure of platinum. The diffraction peak of the 10L-PtRu4/C catalyst are located on the same 2θ as the standard Pt/C catalyst, whereas the diffraction peak of the PtRu4/C catalyst are shifted towards

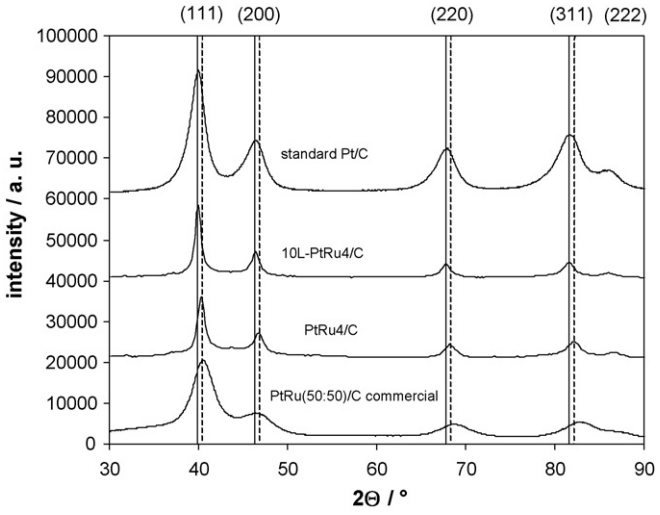

Fig. 4. XRD diffractograms obtained with standard Pt/C, codeposited PtRu4/C, 10L-PtRu4/C and a commercial (Alfa aesar) PtRu (50:50)/C in 2θ range from 30 to 90°.

higher 2θ values. This fact can be related either to PtRu alloy formation or to size effect. But, the apparent crystallites sizes determined by TEM are close for both standard and sputtered catalyst and could not explain the shift of the peaks. These diffraction peaks are located very close to those obtained with a commercial alloyed PtRu (50:50)/C, confirming the formation of PtRu alloy. Therefore, the plasma sputtering technique may produce either alloyed or non-alloyed PtRu structure, according to the preparation method.

3.2. Fuel cell tests with Pt/C anodes

Three anodes with different platinum loadings (0.04/0.08/0.17 mg cm^{-2}) were prepared under similar plasma conditions (Pt deposition rate of 7 μg cm^{-2} min^{-1}) except for the deposition time (6, 11 and 27 min, respectively). Each electrode was hot pressed with a standard cathode (2 mg cm^{-2} Pt loading) against a Nafion® 117 membrane. Fig. 5a compares the cell electrical performance with that of a classical MEA fitted with standard electrodes. The sputtered anodes lead to lower electrical performances than classical assembly in term of achieved current densities at a given cell voltage. The open circuit voltages (ocv) as well as the achieved power densities decrease with the decrease of platinum loading. However, the apparent cell resistance seem to be unaffected by the platinum loading, as the slope at medium current, i.e. in the linear part of the $V(j)$ polarization curves, does not change. Even if the porosity of the electrode surface slightly decreases, due to increase of the platinum loading, no voltage drop at high current density due to fuel transport is visible. Moreover, the platinum particles size determined for standard and sputtered catalysts were of the same order: 2.7 and 2.9–3.0 nm, respectively. It can be assumed that no size effects are involved in the methanol electrooxidation activity of the catalysts. It seems then that only the variation of platinum loading affects the activation of methanol electrooxidation reaction.

Although the platinum loading in catalyst Pt1 is more than 10 times lower than that of the standard anode, the cell performance is only slightly lower. For example, at a current density of 100 mA cm^{-2}, the achieved power densities are close to 25 and 35 mW cm^{-2}, respectively. This fact clearly indicates that the platinum utilization efficiency in the former electrode is at least five times higher than that in the standard electrode. The efficiency of the anode catalyst can be determined by dividing the power output of each cell by the amount of anode catalyst. Results are expressed in mW $mg_{Pt}{}^{-1}$ and plotted as a function of the current density in Fig. 5b. At a cell voltage of 0.1 V, the achieved specific power density reaches 45 mW $mg_{Pt}{}^{-1}$ with standard electrode, 150 mW $mg_{Pt}{}^{-1}$ with the Pt1 anode (0.17 mg_{Pt} cm^{-2}) and 210 mW $mg_{Pt}{}^{-1}$ g with the Pt3 anode (0.04 mg_{Pt} cm^{-2}). The specific activity of sputtered electrodes decreases drastically as the Pt loading increases. This effect can be due to the decrease of the active surface area of platinum with the increase of loading, as it is the case with platinum nanoparticles [45]. Therefore, if the catalyst loading has to be increased to enhance the electrical performance (expressed in mW cm^{-2}), it may be that the specific activity of the sputtered electrode becomes worse than that of a standard electrode. However, concerning the sputtered electrode, increasing the platinum loading leads to decrease the platinum utilization efficiency. Several effects can be proposed to explain the decrease of the specific activity with the increase of the platinum loading.

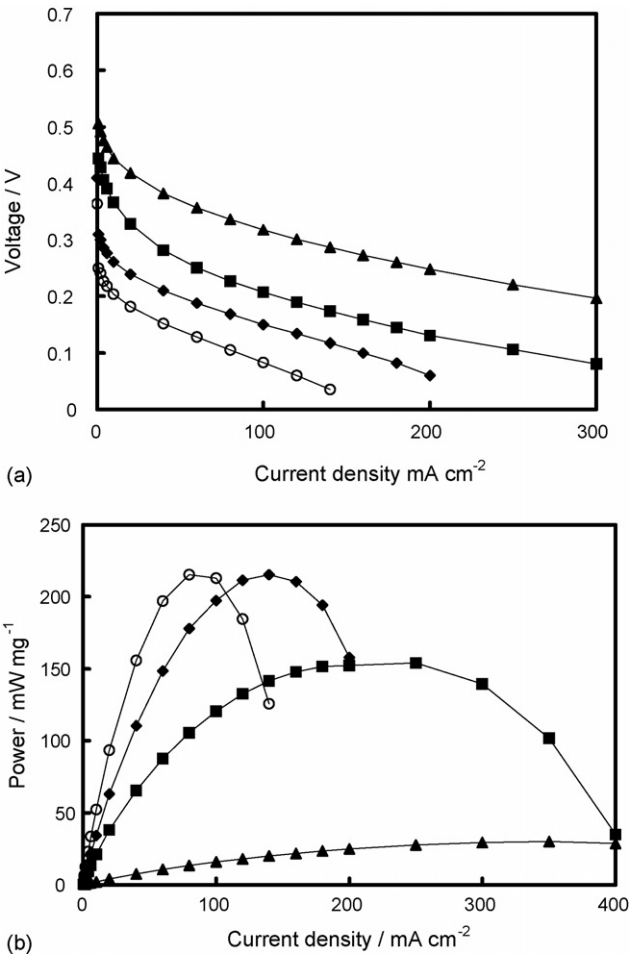

Fig. 5. (a) Cell voltage E vs. current density j curves and (b) specific power vs. current density j in a single 5 cm^2 surface area DMFC with Pt/C anodes with different sputter-deposited loadings of platinum and comparison with a standard anode. Power generator: 100 W; target bias: −300 V; pressure: 0.5 Pa; current on catalytic target: 20 mA; distance target-DL: 5.5 cm. (▲) Standard anode Pt/C 2.0 mg_{Pt} cm^{-2} loading; (■) SPt1 anode Pt/C 0.17 mg cm^{-2}; (♦) SPt2 anode Pt/C 0.08 mg cm^{-2}; (◯) SPt3 anode Pt/C 0.04 mg cm^{-2}. (C_{MeOH} = 2 M; P_{MeOH} = 2 bar; MeOH flow = 2 mL min^{-1}; P_{O_2} = 3 bar; O_2 flow = 120 mL min^{-1}, T_{cell} = 90 °C, membrane Nafion® 117).

First, it may be partly due to the repartition of the Pt layer on the electrode surface and bulk. In a previous paper [42], the study of the depth profile of Pt sputtered on a commercial E-TEK DL determined by RBS showed that the increase of the deposition time at constant deposition rate led to increase the loading of platinum (expressed in μg cm^{-2} nm^{-1}) in the first 100 nm thickness of the DL and to deeper penetration of platinum into the DL. The higher amount of platinum close to the Nafion® membrane explains that the electrical performance expressed in mW cm^{-2} increases with the platinum loading, whereas the deeper penetration of platinum in the DL explains that the specific electrical performance expressed in mW $mg_{Pt}{}^{-1}$ decreases

with platinum loading. In the region close to the Nafion® membrane, the three-phase electrochemical reaction zone [46], i.e. electronic conductor (carbon)–catalyst (platinum)–ionic conductor (Nafion®), is likely optimized conversely to that happens in the depth of the DL. The electrical performances depend drastically on the kinetics of processes occurring in this active layer: reagents diffusion towards catalytic sites, electrochemical reaction at catalysts, ionic mass transport through the solid electrolyte and electronic conduction of carbon [47].

Second, the platinum thin film, which is formed for higher platinum loading, is less active towards methanol electrooxidation than nanoparticles as the consequence of its highest poisoning by adsorbed CO species. The role of highly uncoordinated platinum atoms in electrocatalysis was pointed out to explain the enhancement of CO adsorption and oxidation [48,49]. The thin film of platinum can be considered as platinum bulk and then long distance order can be involved in CO adsorption leading to a saturated coverage of the platinum surface. Malevich et al. [50] have recently shown that CO oxidation proceed at higher overpotential at bulk platinum than at Pt nanoparticles and explained this fact by a change in electrooxidation mechanism.

A lot of investigations are still necessary to determine the optimal loading and depth distribution of catalysts to enhance the cell electrical performance. Many simulation works about PEMFC emphasize a gradient of catalytic sites concentration in the active layer of the electrodes in order to improve platinum catalytic efficiency [32,42,51–53].

3.3. Determination of the electrical performances of sputtered PtRu/C anodes

DMFC working with platinum anodes displayed in all case a drastic voltage drop at low current densities. This is due to poisoning of catalytic surface by CO species coming from dissociative adsorption of methanol at platinum. The modification of platinum catalysts with ruthenium partially prevents the poisoning by CO species, leading to lower the overpotential of methanol electrooxidation and to increase the cell voltage.

Fig. 6 shows the polarisation curves obtained in single 5 cm^2 DMFCs working with 2L-PtRu2/C, 2L-PtRu4/C and Pt3/C electrodes. Adding ruthenium layer to the platinum layer has no effect on the open circuit voltage, conversely to that was expected. Moreover, the apparent cell resistance determined from the slope of the linear region of the $V(j)$ curves at relatively high current density (i.e. low cell voltages corresponding to high anode potentials) increases with the ruthenium loading from 0.6 Ω cm^2 for the Pt3/C anode to 0.8 Ω cm^2 for 2L-PtRu2/C and 1.2 Ω cm^2 for 2L-PtRu4/C anodes. As the main result, double layer Pt/Ru morphology does not lead to an increase of DMFC performance.

Fig. 7 compares the $E(j)$ curves obtained using 10-layer PtRu/C and PtRu/C anodes with a standard Pt/C anode. Conversely to that was observed with double layer PtRu catalysts, 10-layer PtRu catalysts lead to electrical performance

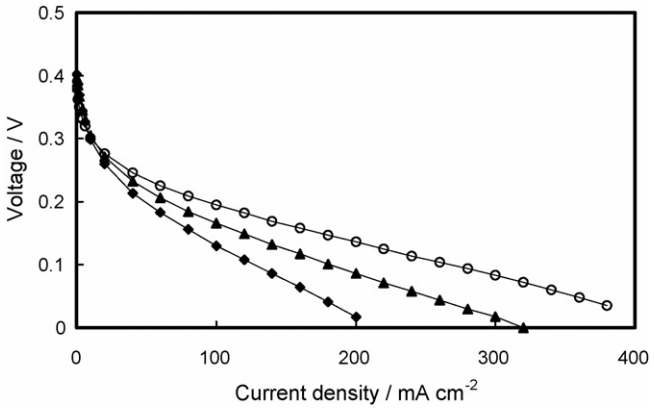

Fig. 6. Cell voltage E vs. current density j in a single 5 cm^2 surface area DMFC working with sputtered PtRu/C anodes (double catalytic layer) of different PtRu loadings. Power generator: 200 W; target bias: −300 V; pressure: 0.5 Pa; current on catalytic target: 20 mA; distance target-DL: 5.5 cm. (◯) Pt/C; 0.4 mg_{Pt} cm^{-2}; (▲) PtRu(86:14)/C; 0.4 mg_{Pt} cm^{-2} and 0.033 mg_{Ru} cm^{-2}; (♦) PtRu(60:40)/C; 0.4 mg_{Pt} cm^{-2} and 0.13 mg_{Ru} cm^{-2}. (C_{MeOH} = 2 M; P_{MeOH} = 2 bar; MeOH flow = 2 mL min^{-1}; P_{O_2} = 3 bar; O_2 flow = 120 mL min^{-1}, T_{cell} = 90 °C, membrane Nafion® 117).

higher than that obtained with Pt/C catalyst, at least in the range from 0 to 250 mA cm^{-2}. However, alloyed PtRu2 and 4 catalysts display the best electrical performance than the 10-layer catalysts 10L-PtRu2 and 4 over the whole studied current density range, independently of the atomic composition. Moreover, ruthenium-poor catalysts always displayed lower electrochemical activity towards methanol electrooxidation than ruthenium rich catalysts.

Alloyed PtRu catalysts with different Pt/Ru atomic ratio were then studied in order to determine the best ratio. Fig. 8 shows the $V(j)$ and $P(j)$ curves obtained in a 5 cm^2 DMFC. The maximum power densities were achieved with catalysts of 70:30 and

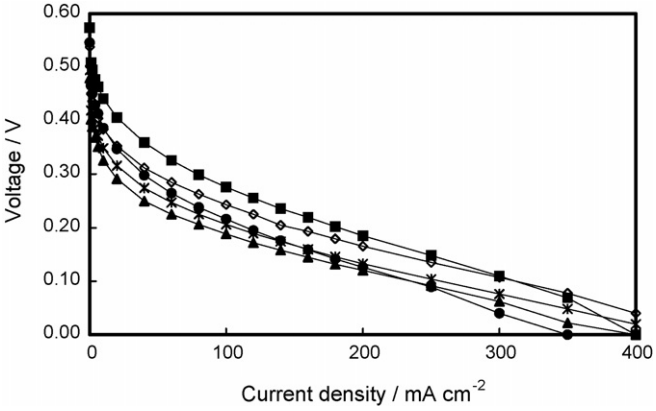

Fig. 7. Cell voltage E vs. current density j in a single 5 cm^2 surface area DMFC working with different PtRu/C anodes. Power generator: 200 W; target bias: −300 V; pressure: 0.5 Pa; current on catalytic target: 20 mA; distance target-DL: 5.5 cm. (▲) sputtered anode Pt/C; 0.3 mg_{Pt} cm^{-2}; (*) 10-layer PtRu(80:20)/C; 0.29 mg_{Pt} cm^{-2} and 0.04 mg_{Ru} cm^{-2}; (♦) 10-layer PtRu(60:40)/C; 0.28 mg_{Pt} cm^{-2} and 0.09 mg_{Ru} cm^{-2}; (◊) "alloy" PtRu(80:20)/C; 0.26 mg_{Pt} cm^{-2} and 0.03 mg_{Ru} cm^{-2}; (■) "alloy" PtRu(60:40)/C; 0.30 mg_{Pt} cm^{-2} and 0.09 mg_{Ru} cm^{-2}. (C_{MeOH} = 2 M; P_{MeOH} = 2 bar; MeOH flow = 2 mL min^{-1}; P_{O_2} = 3 bar; O_2 flow = 120 mL min^{-1}, T_{cell} = 90 °C, membrane Nafion® 117).

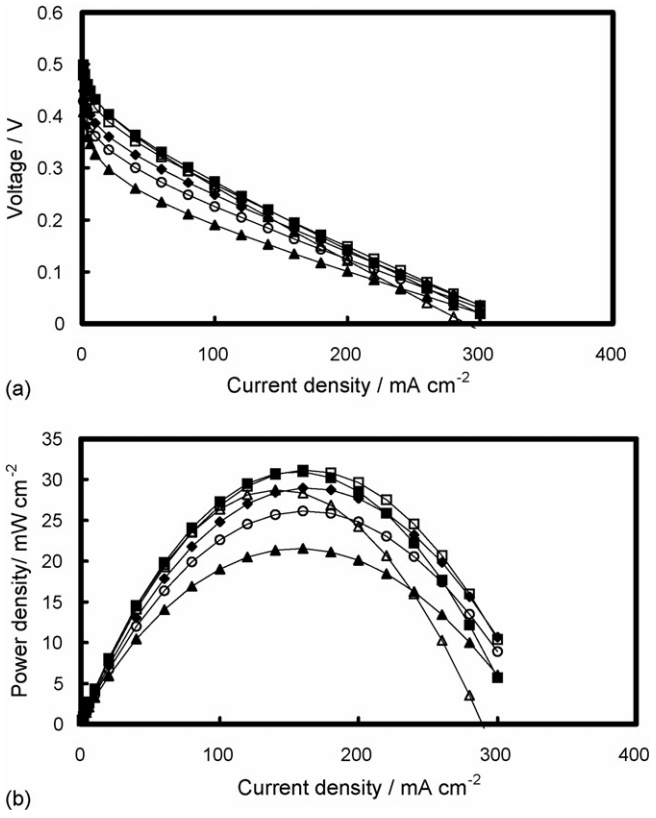

Fig. 8. (a) Cell voltage E vs. current density j curves and (b) power density P vs. current density j in a single 5 cm^2 surface area DMFC working with sputtered PtRu/C anode of different Pt/Ru atomic ratios. Power generator: 200 W; target bias: −300 V; pressure: 0.5 Pa; current on catalytic target: 20 mA; distance target-DL: 5.5 cm. (▲) Pt/C; 0.3 mg$_{Pt}$ cm^{-2}; (◯) PtRu(90:10)/C; 0.32 mg$_{Pt}$ cm^{-2} and 0.02 mg$_{Ru}$ cm^{-2}; (♦) PtRu(80:20)/C; 0.26 mg$_{Pt}$ cm^{-2} and 0.03 mg$_{Ru}$ cm^{-2}; (□) PtRu(70:30)/C; 0.31 mg$_{Pt}$ cm^{-2} and 0.07 mg$_{Ru}$ cm^{-2}; (■) PtRu(60:40)/C; 0.30 mg$_{Pt}$ cm^{-2} and 0.09 mg$_{Ru}$ cm^{-2}; (ρ) PtRu(50:50)/C; 0.33 mg$_{Pt}$ cm^{-2} and 0.17 mg$_{Ru}$ cm^{-2}. (C_{MeOH} = 2 M; P_{MeOH} = 2 bar; MeOH flow = 2 mL min^{-1}; P_{O_2} = 3 bar; O$_2$ flow = 120 mL min^{-1}, T_{cell} = 90 °C, membrane Nafion® 117).

60:40 atomic ratio. However, the best Pt/Ru ratio is depending on desired working point of the cell (i.e. current density and cell voltage). Up to 150 mA cm^{-2}, maximum power density is obtained for Ru atomic ratio of 40%, whereas between 150 and 275 mA cm^{-2}, the best ratio reaches 30%.

Several insights can be drawn from these results. First, the double layer deposition of Pt and Ru leads to the worse fuel cell electrical performances, notably due to the increase of cell apparent resistance. However, Lasch et al. [54] have recently shown that the electric conductivity of RuO_2 materials was comparable to that observed for Vulcan XC-72. The increase of resistivity could also be due to the barrier for protons transfer that is created by the ruthenium layer between the platinum layer (where the methanol dissociative adsorption into CO species occurs) and the electrolytic Nafion® membrane, leading to the appearance of a higher electrical resistance. In the case of 10-layer deposition, the thinner ruthenium layers would not interfere with protons transfer. Second, the alloyed catalysts obtained by co-deposition of Pt and Ru (as determined by XRD) displayed best catalytic activity towards methanol electrooxidation. This result was disappointing for us because with multiplayer deposition, a structure close to platinum decorated by ruthenium was expected. It was shown by different authors that this catalyst structure leads to enhance catalytic activity towards methanol electrooxidation [40,55]. However, it is likely that under our experimental conditions of multi-layer catalysts preparation, a ruthenium shell is formed on platinum particles, limiting the electrocatalytic activity. At last, because ruthenium activates water molecules at lower potentials than platinum, the presence of large amount of ruthenium leads to the best activity at higher cell voltages. However, at lower cell voltages, platinum rich catalysts become the most active ones. According to Watanabe et al. [56], in the limiting current range of methanol oxidation at ruthenium-rich catalysts, the catalytic surface is blocked by adsorbed oxygen species, which makes the adsorption of organic species more difficult. On the other hand, according to Gasteiger et al. [57], for anode potentials greater than 0.5 V/RHE, i.e. lower cell voltages, pure platinum displays a greater activity than ruthenium for methanol oxidation. The combination of both effects explains the decrease in cell performances with the increase of the ruthenium atomic ratio. In previous works [26,31] where anodes were prepared either via a colloidal route (non-alloyed catalysts) or an electrochemical method (alloyed catalysts), the best Pt/Ru bulk ratio in terms of higher achieved power density of the DMFC was (80:20), whereas in this study, the Pt/Ru bulk ratio is a little bit higher (70:30). This indicate that the preparation method of bimetallic catalysts with the same bulk Pt/Ru atomic ratio influence definitely the surface composition, and further its electroactivity towards methanol oxidation, i.e. the fuel cell electrical performances. Unfortunately, it is also a very challenging experimental problem to determine the surface composition of non-well-defined catalytic surface, so that only bulk composition can be compared.

4. Conclusion

Low metal loading catalysts for methanol electrooxidation were prepared by plasma sputtering technique. The activity of the sputtered catalyst on a gas diffusion layer is lower than that obtained with a standard anode. However, the specific activity is much higher, indicating that the efficiency of use of the sputtered platinum catalysts is higher than that of a chemical electrode. However, platinum activity decreases when catalyst loading increases on the DL, likely due to the repartition of the Pt layer on the electrode surface and bulk, and to the formation of a thin platinum film on the top of the DL. Ruthenium was deposited with platinum by sputtering. The best efficiency is reached when both metals are simultaneously deposited (alloy formation) with a ruthenium atomic ratio of 30% or 40%$_{Ru}$ depending of the working voltage of the cell. But DMFC electrical performances remain lower than that obtained with standard MEAs.

However, this study showed that plasma sputtering was a powerful method to prepare and control the composition and structure of multi-metallic catalysts. It allows varying easily synthesis parameters (notably the decrease of either deposition time or power in the case of multiplayer, the increase of the number

of layers, order of the layers. . .) in order to optimize the catalysts structure and activity. For example, increasing the number of layers for a given total loading of catalyst (i.e. decreasing the metal amount deposition in each layer) may avoid the formation of thin platinum film (less active for methanol electrooxidation) and may lead to real decoration of platinum layer by ruthenium islands. Both these effects could enhance the catalyst activity. Bimetallic catalysts are also interesting to decrease the platinum loading of the cathode or to protect the anode from CO poisoning. This technology could then be used in the field of PEMFCs, where the catalyst loading is lower than in DAFC electrodes, which could prevent the risk of the decrease of the specific activity.

Acknowledgements

The authors acknowledge the CNRS 'Programme Energie' and "Actions Concertées Incitatives" for financial support. We would like to thank two experts for surface analysis: Y. Tessier from CERI (Orléans, France) and T. Cacciagerra from CRMD (Orléans, France) for assistance with respectively RBS and TEM measurements. G. Coudrat is acknowledged for precious technical help.

References

[1] R. Nolte, J. Power Sources 4573 (2001) 1.
[2] M. Wang, J. Power Sources 112 (2002) 307.
[3] D. Chu, R. Jiang, K. Gardner, R. Jacobs, J. Schmidt, T. Quakenbush, J. Stephens, J. Power Sources 96 (2001) 174.
[4] A. Heinzel, C. Hebling, M. Müller, M. Zedda, C. Müller, J. Power Sources 105 (2002) 250.
[5] S. Baranton, C. Coutanceau, J.-M. Léger, C. Roux, P. Capron, Electrochim. Acta 51 (2005) 517.
[6] G.J.K. Acres, J. Power Sources 100 (2001) 60.
[7] J. Hamelin, K. Agbossou, A. Laperrière, F. Laurencelle, T.k. Bose, Int. J. Hydrogen Energy 26 (2001) 625.
[8] P. Costamagna, S. Srinivasan, J. Power Sources 102 (2001) 253.
[9] J.W. Gosselink, Int. J. Hydrogen Energy 27 (2002) 1125.
[10] N. Takeichi, H. Senoh, T. Yokota, H. Tsuruta, K. Hamada, H.T. Takeshita, H. Tanaka, T. Kiyobayashi, T. Takano, N. Kuriyama, Int. J. Hydrogen Energy 28 (2003) 1121.
[11] R. Ströbel, M. Oszcipok, M. Fasil, B. Rohland, L. Jörissen, J. Garche, J. Power Sources 105 (2002) 208.
[12] C. Lamy, J.-M. Léger, J. Phys. IV 4 (1994) C1.
[13] T. Iwasita, H. Hoster, A. John-Anaker, W.F. Lin, W. Vielstich, Langmuir 16 (2000) 522.
[14] M. Krausa, W. Vielstich, J. Electroanal. Chem. 379 (1994) 307.
[15] M. Watanabe, S. Motoo, J. Electroanal. Chem. 60 (1975) 275.
[16] T. Frelink, W. Visscher, J.A.R. Van Veen, Langmuir 12 (1996) 3702.
[17] C. Lu, C. Rice, M.I. Masel, P.K. Babu, P. Waszczuk, H.S. Kim, E. Oldfield, A. Wieckowski, J. Phys. Chem. B 106 (2002) 958.
[18] P. Waszczuk, A. Wieckowski, P. Zelenay, S. Gottesfeld, C. Coutanceau, J.M. Léger, C. Lamy, J. Electroanal. Chem. 511 (2001) 55.
[19] A.K. Shukla, P.A. Christensen, A.J. Dickinson, A. Hamnett, J. Power Sources 76 (1998) 54.
[20] S.C. Thomas, X. Ren, S. Gottesfeld, J. Electrochem. Soc. 146 (1999) 4354.
[21] P. Argyropoulos, K. Scott, W.M. Taama, J. Power Sources 87 (2000) 152.
[22] A. Fisher, J. Jindra, H. Wendt, J. Appl. Electrochem. 28 (1998) 277.
[23] P.L. Antonucci, A.S. Arico, P. Creti, E. Ramunni, V. Antonucci, Solid-State Ionics 125 (1999) 431.
[24] S. Lister, G. McLean, J. Power Sources 130 (2004) 61.
[25] V. Mehta, J.S. Cooper, J. Power sources 114 (2003) 32.
[26] L. Dubau, C. Coutanceau, E. Garnier, J.-M. Léger, C. Lamy, J. Appl. Electrochem. 33 (2003) 419.
[27] S. Rousseau, C. Coutanceau, E. Lamy, J.-M. Léger, J. Power Sources. 158 (2006) 18.
[28] F. Gloaguen, J.-M. Léger, C. Lamy, A. Marmann, U. Stimming, R. Vogel, Electrochim. Acta 44 (1999) 1805.
[29] S.D. Thomson, L.R. Jordan, M. Forsyth, Electrochim. Acta 46 (2001) 1657.
[30] K.H. Choi, H.S. Kim, T.H. Lee, J. Power Sources 75 (1998) 230.
[31] C. Coutanceau, A.F. Rakotondrainibé, A. Lima, E. Garnier, S. Pronier, J.-M. Léger, C. Lamy, J. Appl. Electrochem. 34 (2004) 61.
[32] P. Brault, A. Caillard, A.L. Thomann, J. Mathias, C. Charles, R.W. Boswell, S. Escribano, J. Durand, T. Sauvage, J. Phys. D: Appl. Phys. 37 (2004) 3419.
[33] S. Hirano, J. Kim, S. Srinivasan, Electrochim. Acta 42 (1997) 1587.
[34] S.Y. Cha, W.M. Lee, J. Electrochem. Soc. 146 (1999) 4055.
[35] R. O'Hayre, S.J. Lee, S.W. Cha, F.B. Prinz, J. Power Sources 109 (2002) 483.
[36] A.T. Haug, R.E. White, J.W. Weidner, W. Huang, S. Shi, T. Stoner, N. Rana, J. Electrochem. Soc. 149 (2002) A280.
[37] L. Mex, N. Ponath, J. Müller, Fuel Cell Bull. 39.
[38] C.K. Witham, W. Chun, T.I. Valdez, S.R. Narayama, Electrochem. Solid-State Lett. 3 (2000) 497.
[39] H. Bönnemann, W. Brijoux, R. Brinkmann, R. Fretzen, T. Joussen, R. Köppler, B. Korall, P. Neiteler, J. Richter, J. Mol. Catal. 86 (1994) 129.
[40] L. Dubau, F. Hahn, C. Coutanceau, J.-M. Léger, C. Lamy, J. Electroanal. Chem. 554/555 (2003) 407.
[41] L. Demarconnay, C. Coutanceau, J.-M. Léger, Electrochem. Acta 49 (2004) 4513.
[42] A. Caillard, P. Brault, J. Mathias, C. Charles, B.W. Boswell, T. Sauvage, Surf. Coat. Technol. 200 (2005) 391.
[43] L. Dubau, PhD thesis, University of Poitiers 2003.
[44] W. Vogel, P. Britz, H. Bönnemann, J. Rothe, J. Hormes, J. Phys. Chem. B 101 (1997) 11029.
[45] A.A. Mikhaylova, O.A. Khazova, V.S. Bagotzky, J. Electroanal. Chem. 480 (2000) 225.
[46] K. Kinoshita, Electrochemical Oxygen Technology, John Wiley and Sons, New York, 1992, p. 174.
[47] S. Motoo, M. Watanabe, N. Furuya, J. Electroanal. Chem. 160 (1984) 351.
[48] C. Lemire, R. Meyer, S. Shaikhutdinov, H.-J. Freund, Angew. Chem. Int. Ed. 43 (2004) 118.
[49] N.P. Lebedeva, A. Rodes, J.-M. Feliu, M.T.M. Koper, R.A. van Santen, J. Phys. Chem. B 106 (2002) 9863.
[50] D. Malevich, J. Li, M.K. Chung, C. McLaughlin, M. Schlaf, J. Lipkowski, J. Solid-State Electrochem. 9 (2005) 267.
[51] D. Song, Q. Wang, Z. Liu, T. Navessin, S. Holdcroft, Electrochim. Acta 50 (2004) 725.
[52] O. Antoine, Y. Bultel, P. Ozil, R. Durand, Electrochim. Acta 45 (2000) 4493.
[53] Z.N. Farhat, J. Power Sources 138 (2004) 68.
[54] K. Lasch, G. Hayn, L. Jörissen, J. Garche, O. Besenhardt, J. Power Sources 105 (2002) 305.
[55] P. Waszczuk, J. Solla-Gullón, H.-S. Kim, Y.Y. Tong, V. Montiel, A. Aldaz, A. Wieckowski, J. Catal. 203 (2001) 1.
[56] M. Watanabe, S. Motoo, J. Electroanal. Chem. 60 (1975) 267.
[57] H.A. Gasteiger, N. Markovic, P.N. Ross, E.J. Cairns, J. Electrochem. Soc. 141 (1994) 1795.